LIMNOLOGY and OCEANOGRAPHY

ASLO

Limnol. Oceanogr. 9999, 2024, 1–16

doi: 10.1002/lno.12683

High-frequency sampling captures variability in phytoplankton population-specific periodicity, growth, and productivity

Annette M. Hynes,[1] **Jordan Winter**,[1] **Chris T. Berthiaume**,[1] **Eric Shimabukuro**,[2] **Kelsy Cain**,[1] **Angelicque White**,[2] **E. Virginia Armbrust**,[1] **François Ribalet**[1*]

[1]School of Oceanography, University of Washington, Seattle, Washington, USA
[2]School of Ocean and Earth Science and Technology, University of Hawaii, Mānoa, Hawaii, USA

Abstract

The Hawaii Ocean Time-series (HOT) at Station ALOHA (22.75°N, 158°W) in the North Pacific Subtropical Gyre (NPSG) serves as a critical vantage point for observing plankton biomass production and its ecological implications. However, the HOT program's near-monthly sampling frequency does not capture shorter time scale variability in phytoplankton populations. To address this gap, we deployed the SeaFlow flow cytometer for continuous monitoring during HOT cruises from 2014 to 2021. This approach allowed us to examine variations in the surface abundance and cell carbon content of specific phytoplankton groups: the cyanobacteria *Prochlorococcus*, *Synechococcus*, and *Crocosphaera* as well as a range of small eukaryotic phytoplankton ($\leq 5\,\mu$m). Our data showed that daily to monthly variability in *Prochlorococcus* and *Synechococcus* abundance matches seasonal and interannual variability, while small eukaryotic phytoplankton and *Crocosphaera* showed the highest seasonal and interannual fluctuations. The study also found that eukaryotic phytoplankton and *Crocosphaera* had higher median cellular growth rates (0.076 and 0.090 h^{-1}, respectively) compared to *Prochlorococcus* and *Synechococcus* (0.037 and 0.045 h^{-1}, respectively). These variances in abundance and growth rates indicate that shifts in the community structure significantly impact primary productivity in the NPSG. Our results underscore the importance of daily to monthly phytoplankton dynamics in ecosystem function and carbon cycling.

The North Pacific Subtropical Gyre (NPSG) plays a critical role in global biogeochemical cycles, representing one of the oldest and largest ecosystems on the planet. Since 1988, the Hawaii Ocean Time-series (HOT) program has characterized the seasonal and interannual variability of phytoplankton community structure and primary production during near-monthly cruises at Station ALOHA (A Long-term Oligotrophic Habitat Assessment), a location representative of the NPSG (Karl and Lukas 1996; Karl et al. 2021). These nutrient-poor waters are numerically dominated by the cyanobacteria *Prochlorococcus* and *Synechococcus* and eukaryotic picophytoplankton (< 2 μm) (Campbell et al. 1997). In the surface mixed layer, where the highest rates of primary production occur (Karl et al. 2021), *Prochlorococcus* abundance remains fairly constant throughout the year, while *Synechococcus* abundance peaks in winter (December–February), picoeukaryotes in spring (March–May), and the unicellular N_2-fixing cyanobacterium *Crocosphaera* in late summer to early fall (July–September) (Campbell et al. 1994, 1997; Church et al. 2009). Most of the variability in surface primary production is subseasonal (64%), with less variability at the seasonal (11%), interannual (23%), or long-term time scales (2%) (Karl et al. 2021).

There is increasing evidence that episodic events that occur on the time scale of days to weeks affect the metabolic state of the NPSG (Barone et al. 2019a, 2022; Henderikx-Freitas et al. 2020; Rii et al. 2022). While the euphotic zone typically maintains metabolic balance where primary production equals community respiration (Ferrón et al. 2015; Barone et al. 2019b), measurements made during consecutive days show pulses in net community and primary productivity (Ferrón et al. 2015; Wilson et al. 2015). These pulses can be linked to episodic processes such as mixing events that shoal the nitracline and bring new nitrogen into the euphotic zone

*Correspondence: ribalet@uw.edu

Additional Supporting Information may be found in the online version of this article.

Author Contribution Statement: AMH: Conceptualization, Data Curation, Formal Analysis, Methodology, Visualization, Writing – Original Draft, Writing – Review & Editing. JW: Formal Analysis, Writing – Review & Editing. CTB: Software, Formal Analysis, Writing – Review & Editing. ES: Formal Analysis. KC: Formal Analysis, Writing – Review & Editing. AW: Funding Acquisition, Resources, Writing – Review & Editing. EVA: Funding Acquisition, Resources, Conceptualization, Writing – Original Draft, Writing – Review & Editing. FR: Funding Acquisition, Resources, Conceptualization, Validation, Supervision, Writing – Original Draft, Writing – Review & Editing.

and stimulate export production (Karl et al. 1996); mesoscale eddies and Rossby waves that uplift nutrients into the photic zone and stimulate phytoplankton blooms of haptophytes and pelagophytes (Sakamoto et al. 2004; Karl and Church 2014); and summer and fall shallowing of the mixed layer depths and mesoscale eddies that cause N_2-fixing blooms of *Trichodesmium*, *Richelia*–diatom symbioses, and *Crocosphaera* (Letelier and Karl 1996; White et al. 2007; Dore et al. 2008; Fong et al. 2008; Dugenne et al. 2023).

The daily light cycle also plays an important role in primary production, synchronizing photosynthetic parameters (Xie et al. 2018) and phytoplankton cell division (Vaulot et al. 1995; Jacquet et al. 2001) and leading to daily fluctuations in phytoplankton cell size, biomass, cell division rates (Ribalet et al. 2015; Li et al. 2022a), and bulk particle concentrations (White et al. 2017; Henderikx-Freitas et al. 2020). In addition to photosynthesis, the day/night cycle affects the timing of N_2 fixation in *Crocosphaera* (Wilson et al. 2017; Masuda et al. 2018). This diurnal variability cascades to the rest of the community via fluctuating phytoplankton mortality rates (Ribalet et al. 2015) and differential ingestion rates by heterotrophic protistan grazers (Connell et al. 2020).

To capture diel, seasonal, and interannual variations in phytoplankton biomass and productivity at Station ALOHA, we deployed SeaFlow, a custom-built shipboard flow cytometer (Swalwell et al. 2011), during 42 research cruises between December 2014 and January 2021. The cytometer continuously measured the individual cell properties of *Prochlorococcus*, *Synechococcus*, *Crocosphaera*, and small eukaryotic phytoplankton, allowing us to infer hourly growth rates and net productivity. We hypothesized that abundances would correlate with cellular growth rates in seasonal populations and that cellular growth rates would show seasonality even in *Prochlorococcus*, known for their stability across seasons. This study underscores the importance of small-scale variability in community structure for regulating primary production in oligotrophic ocean gyres.

Methods

Shipboard flow cytometry

The shipboard flow cytometer SeaFlow (Swalwell et al. 2011) was deployed on 35 HOT cruises and 7 cruises that transited within 0.5° of Station ALOHA (22°45′N, 158°W). SeaFlow sampled continuously from the underway seawater system at a depth of 3–8 m, depending on the ship. The seawater was diverted into an overflowing bucket and from there pumped through a 100-μm stainless steel mesh filter to prevent clogging of the 200-μm sampling nozzle. Then, 1-μm yellow-green Fluoresbrite microspheres (Polysciences, Inc.) were continuously injected into the stream and served as standard beads. Initially, particles were excited by a 300-mW, 457-nm laser, but in December 2019, this was replaced with a laser offering variable wattage (300–500 mW) and a wavelength of 460 nm. We have assessed the impact of this change and determined that it does not affect significantly the data, ensuring continuity and reliability of measurements across the update. Emission was detected by two position-sensitive detectors that determine which particles are in focus and at three wavelength bands: chlorophyll *a* (Chl *a*) fluorescence (692/40-nm bandpass filter), phycoerythrin fluorescence (572/28-nm bandpass filter), and forward light scatter (457/50-nm bandpass filter) (Swalwell et al. 2011). Raw data were stored in 3-min intervals.

Flow cytometry data processing

Raw SeaFlow data were first processed as described in Ribalet et al. (2019) to identify in-focus optimally positioned particles (OPP) within the SeaFlow virtual core (Swalwell et al. 2011). The OPP were then analyzed using the package `popcycle` 4.7.3 in **R** (Ribalet et al. 2019). Five sets of gates were defined based on forward light scatter, Chl *a* fluorescence, and phycoerythrin fluorescence and were applied to all data to identify 1-μm beads, *Prochlorococcus*, *Synechococcus*, small eukaryotic phytoplankton ($\leq$ 5 μm), and *Crocosphaera*. Gate coordinates were saved for each file and stored in a SQL database.

Surface populations of *Prochlorococcus*, characterized by low chlorophyll fluorescence, are detected near the background noise on the SeaFlow, leading to potential underestimation of their abundance. Therefore, abundance of *Prochlorococcus* was calibrated based on cell counts derived from discrete surface samples. Water was collected from Niskin bottles at 5 m depth on each cruise, fixed (0.24% paraformaldehyde, final concentration), and stored at − 80°C. Samples were thawed and run on an Influx flow cytometer (Becton, Dickinson and Company) with excitation by 100 mW, 488 nm and 1 W, 457 nm lasers simultaneously focused at the same pinhole and emission detected at three wavelengths: Chl *a* fluorescence (692/40 nm bandpass filter), phycoerythrin fluorescence (585/40 nm bandpass filter), and forward light scatter (488 nm blocking). Influx-based cell abundances of *Prochlorococcus* were assumed to represent true abundances whereas SeaFlow-based abundances for *Synechococcus*, small eukaryotic phytoplankton, and *Crocosphaera* were assumed to be correct (Supporting Information Fig. S3). The SeaFlow *Prochlorococcus* abundances for each cruise were adjusted by a correction factor c:

$$c = \sum_{t=1}^{N} \frac{X_{\mathrm{in},t}}{N \times \sum_{k=t-1}^{t+1} \left(X_{\mathrm{sf},k}\right)/n}, \quad (1)$$

where $X_{\mathrm{in},t}$ is the *Prochlorococcus* cell abundance estimated by Influx collected at time t, N is the number of Influx samples, $X_{\mathrm{sf},k}$ is the *Prochlorococcus* cell abundances estimated by SeaFlow collected at time $t \pm 1$ h, and n is the number of 3-min SeaFlow samples collected during the period $t \pm 1$ h. Correction factors are available on GitHub in the `popcycle` package (https://github.com/seaflow-uw/popcycle/blob/master/inst/abundance/abundance-calibration.csv).

Equivalent spherical diameter (ESD) of each cell was estimated from forward scatter by the application of Mie light scatter theory based on three refractive indices (1.35, 1.38, and 1.41) that cover the range applicable to marine phytoplankton (Lehmuskero et al. 2018). The choice of refractive index for *Crocosphaera* and small eukaryotic phytoplankton was 1.35. As the scattering intensity can vary based on optical alignment, the choice of refractive index for *Prochlorococcus* and *Synechococcus* was chosen for each cruise based on the closest median ESD to 0.6 μm for *Prochlorococcus* at Station ALOHA (Casey et al. 2019). The refractive indices used for each cruise can be found in our Github repository (https://github.com/seaflow-uw/popcycle/blob/master/inst/scatter/RefracIndices_percruise.csv).

Carbon quota for individual cells was estimated using the ESD to calculate volume-to-carbon relationships for small protists (< 3000 μm^3; Menden-Deuer and Lessard 2000):

$$Q_C = 0.261 \times \text{vol}^{0.860}, \quad (2)$$

where Q_C is carbon quota (pg C cell^{-1}) and vol is the cell volume (μm^3).

Processed SeaFlow data including abundance, diameter, and carbon quota are available in the Zenodo public data repository (doi: 10.5281/zenodo.7154076). Code for analysis is available on GitHub (https://github.com/ANetTow/SeaFlow_ALOHA).

Seasonality

Daily mean abundances for each phytoplankton population were grouped by season: winter (December–February), spring (March–May), summer (June–August), and fall (September–November). A Kruskal–Wallis rank sum test was applied to determine whether abundances from the four seasons came from the same distribution with a significance level of $\alpha < 0.01$. For each phytoplankton group with significant differences among seasonal abundances, a post hoc Dunn test with a significance level of $\alpha < 0.01$ was performed to compare each pair of seasons with a Benjamini–Hochberg adjustment of the p values for multiple comparisons to control the false discovery rate.

Nonparametric periodicity analysis

Twenty-four–hour periodicity of cell abundance and carbon quota were assessed for each phytoplankton population for a given cruise using the Rhythmicity Analysis Incorporating Nonparametric methods (RAIN) implemented in **R** (Thaben and Westermark 2014), which detects the rising and falling of a wave without assumption of its shape. We aggregated the SeaFlow data, originally collected at 3-min intervals, into hourly means prior to analysis, thereby aligning with the optimal input range of 10–100 measurements for effective time-series analysis. This processing step was performed for all cruises, resulting in time points ranging from 33 to 92 h, with a single exception of HOT-322, which presented 138 time points. We controlled for the false discovery rate using the adaptive Benjamini–Hochberg method. Cruises with less than 48 h of data were removed from analysis. The population abundance threshold was 0.02×10^6 cells L^{-1} to ensure that there were at least 30 cells per file to approximate a normal distribution. Cruises with significant periodicity ($p < 0.01$) were used to determine the timing of an abundance minimum or carbon quota maximum.

Biomass, growth rates, and productivity

Biomass (B, μg C L^{-1}) was estimated as:

$$B = \overline{Q_C} \times X, \quad (3)$$

where $\overline{Q_C}$ is population mean carbon quota (pg C cell^{-1}) and X is cell abundance (cells L^{-1}) from SeaFlow data.

We estimated two biomass-based rates; the cellular growth and net carbon productivity rates. The daily net scatter–based cellular growth rate (r, h^{-1}) and the carbon quota at sunrise $Q_{C,0}$ were derived by fitting a transformed exponential growth function:

$$\ln(Q_C) = r \times t + \ln(Q_{C,0}), \quad (4)$$

through hourly mean carbon quota (Q_C, pg C cell^{-1}) where t is the number of hours since sunrise (h). Data were fit from sunrise to sunset as determined by the solar calculator `suncalc` in **R**. To estimate cellular growth rate r, data series had to meet the following three conditions: (1) estimates were based on more than 30 observations per 3-min file (i.e., cell abundance was $\geq 0.02 \times 10^6$ cells L^{-1}), (2) daytime data spanned at least 6 h, and (3) the p value for the rate estimate was ≤ 0.01 to be considered significant. A Kruskal–Wallis rank sum test was applied to determine whether the growth rates for each phytoplankton group came from the same distribution. A post hoc Dunn test with a significance level of $\alpha < 0.01$ was performed to compare each pair of phytoplankton groups to determine which growth rates were significantly different from each other, with a Benjamini–Hochberg adjustment of the p value for multiple comparisons to control the false discovery rate. Net carbon productivity in the absence of cell loss (C_{prod}, μg C L^{-1} d^{-1}) was estimated by:

$$C_{\text{prod}} = X_0 \times Q_{C,0} \times \left(e^{r \times t_d} - 1\right), \quad (5)$$

where t_d is day length (h) calculated by the difference between sunset and sunrise as determined by the solar calculator package `suncalc` in **R**, and X_0 is the abundance at sunrise (cells L^{-1}).

Variability across time scales

Distributions of variability (V) in abundance and cellular growth rate were calculated by the fold change for sequential time steps:

$$V = \frac{|Y_t - Y_{t+1}|}{Y_t}, \quad (6)$$

where Y_t is the abundance or cellular growth rate at time step t, Y_{t+1} is the abundance or cellular growth rate at the subsequent time step, and time step lengths included hourly (abundance only), daily, monthly, seasonally (3 months), and annually. To avoid measuring sequential time steps larger than the intended resolution, for example measuring a "daily" change between two cruises a month apart, time gaps in data were limited to 5 h (hourly), 3 d (daily), 45 d (monthly), and 100 d (seasonal). To test whether variability among time resolutions within each population were from the same distributions, a Kruskal–Wallis rank sum test was applied. For populations with a significant Kruskal–Wallis test, a post hoc Dunn test with a significance level of $\alpha < 0.01$ was performed to compare time-resolved variability between pairs of time scales to determine which scales were significantly different from each other, with a Benjamini–Hochberg adjustment of the p value for multiple comparisons to control the false discovery rate.

Cell abundances for *Prochlorococcus*, *Synechococcus*, and small eukaryotic phytoplankton; Chl *a* concentrations; ^{14}C-based primary productivity; and particulate carbon data for depths < 10 m measured through the Hawaii Ocean Time-series program were obtained via the HOT-DOGS application (https://hahana.soest.hawaii.edu/hot/hot-dogs). Chl *a* concentrations and ^{14}C-based primary productivity were analyzed as described in Karl et al. (2021). Briefly, water samples were collected 3–4 h before dawn from the CTD-rosette sampling system. Triplicate 150 mL samples were collected in dark polyethylene bottles to measure Chl *a* concentrations fluorometrically (Letelier et al. 1996). Subsamples were withdrawn under dim light into two 500-mL polycarbonate bottles and inoculated with $NaH^{14}CO_3$. The bottles were incubated from dawn to dusk, one in light and one in dark, then subsamples were filtered onto 25-mm glass fiber filters (Whatman GF/F), and the filters were placed in a glass vial and frozen until ^{14}C incorporation into particulate matter could be measured by a shore-based scintillation counter. Particulate carbon (PC) was analyzed as described in Karl et al. (2022). Briefly, water samples were collected from the CTD-rosette sampling system and filtered onto precombusted 25-mm glass fiber filters (Whatman GF/F), placed in combusted foil in polystyrene dishes, and stored frozen until dried and pressed into a pellet for elemental analysis.

Results

Abundance

SeaFlow was used at Station ALOHA to continuously measure cyanobacteria—specifically *Prochlorococcus*, *Synechococcus*, and *Crocosphaera*—as well as the small eukaryotic phytoplankton with an equivalent spherical diameter less than 5 μm (Supporting Information Fig. S1). The instrument yielded 150 d of data (Supporting Information Table S1; Fig. S2).

The daily average cell abundance varied day to day, with significant month-to-month and year-to-year fluctuations in *Prochlorococcus* and *Synechococcus* abundances, irrespective of whether the data were obtained with SeaFlow or were single-point measurements from the HOT program at Station ALOHA (Fig. 1). *Prochlorococcus* showed no significant seasonal variance in median abundance ($p = 0.11$, Kruskal–Wallis test), whereas *Synechococcus*, the small eukaryotes, and *Crocosphaera* each displayed seasonal trends ($p < 0.01$, Kruskal–Wallis test; Table 1). Specifically, *Synechococcus* abundance increased significantly in winter and spring ($p < 0.01$, Dunn test), small eukaryotes were more abundant in winter–spring compared to fall ($p < 0.01$, Dunn test), and *Crocosphaera* showed higher abundance in summer and fall ($p < 0.01$, Dunn test; Table 1). During four summer cruises, small eukaryotic phytoplankton and *Crocosphaera* displayed blooms, defined as instances where abundance was two standard deviations above the mean, with these blooms co-occurring during three cruises. Interestingly, while SeaFlow measurements generally aligned with the HOT data collected from Niskin bottles at 5-m depth (Supporting Information Fig. S3), these summer blooms went undetected by the HOT program.

Diel variability in phytoplankton abundance was evident throughout the time series. We analyzed 31 cruises that featured at least 48 h of SeaFlow data to assess the synchronization of hourly abundance fluctuations with the day/night cycle. A significant 24-h periodicity in cell abundance ($p < 0.01$) was consistently detected for at least one phytoplankton population on each cruise, so there were no instances where all populations showed a lack of periodicity (Fig. 2). Although *Prochlorococcus* displayed morning (06:00–09:00) abundance minima during 29% of the cruises, the timing of daily abundance minima was otherwise remarkably consistent; 45% of *Prochlorococcus*, 48% of *Synechococcus*, and 52% of small eukaryotic phytoplankton time series reached their lowest hourly abundance toward dusk and early evening (16:00–22:00), while 58% of *Crocosphaera* abundance minima occurred near or after dawn (04:00–10:00; Fig. 2). These results emphasize the strong diel synchrony among phytoplankton populations.

Diel variation in diameter and carbon quota

As seen in abundance, diel changes in equivalent spherical diameter and carbon quota (i.e., carbon per cell) for each phytoplankton population were synchronized with the day/night cycle (Fig. 3; Supporting Information Fig. S4). *Prochlorococcus*, *Synechococcus*, and small eukaryotic phytoplankton displayed peaks in hourly carbon quota in the hours around dusk (16:00–21:00), while most periodic *Crocosphaera* time series peaked later in the evening (20:00–00:00) (Supporting Information Fig. S4). For 45% of the cruises, *Crocosphaera* carbon quota was aperiodic, and in each of these cases, abundance was low ($\leq 0.02 \times 10^6$ cells L^{-1}). Conversely, for 19% of the cruises, *Crocosphaera* carbon quota was significantly periodic despite low abundances. We calculated the absolute ranges

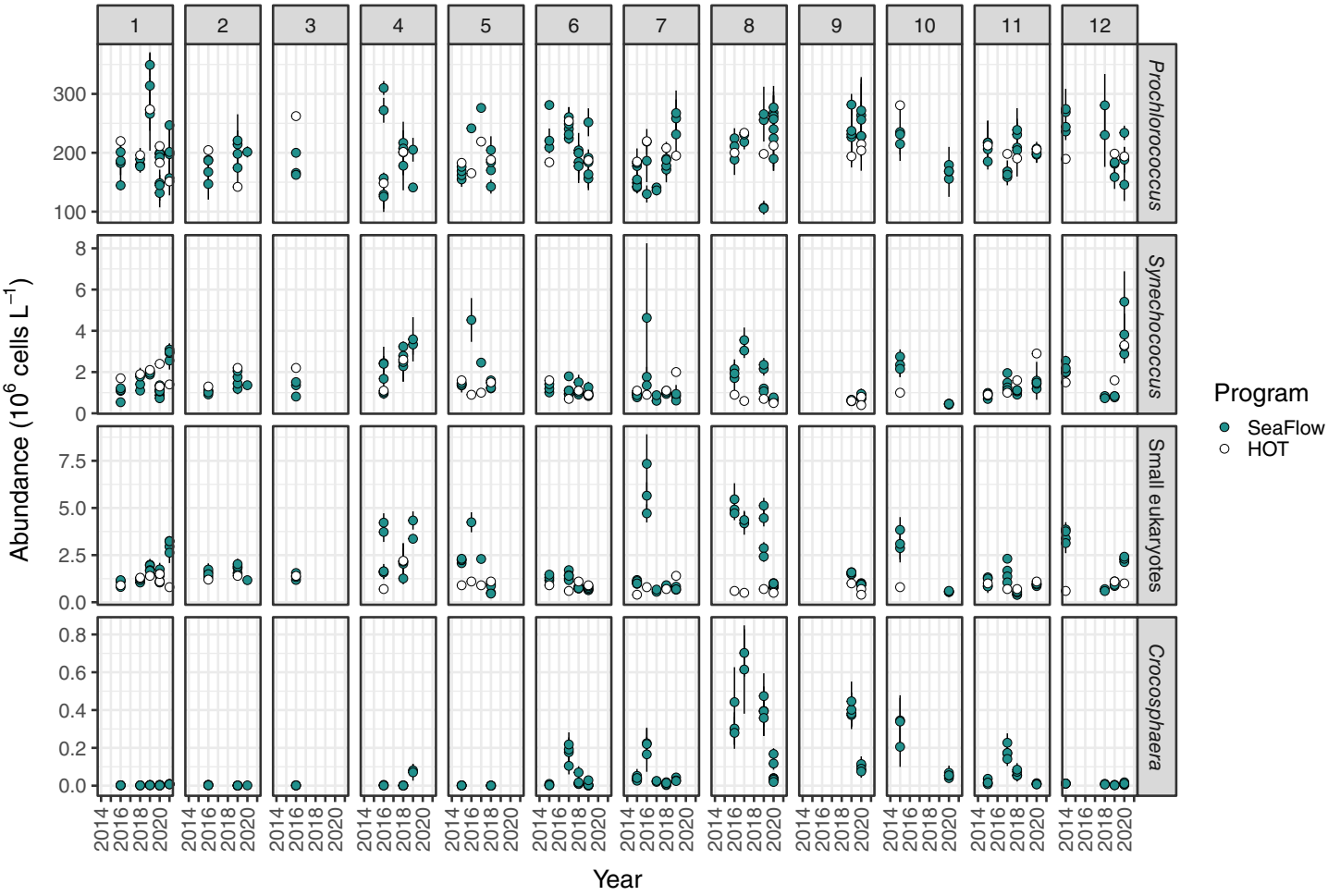

Fig. 1. Daily mean abundances of *Prochlorococcus*, *Synechococcus*, small eukaryotic phytoplankton, and *Crocosphaera* populations determined via SeaFlow (teal circles) or derived from the Hawaii Ocean Time-series (HOT) program (5 m, white circles). Error bars for SeaFlow data indicate standard deviation calculated from hourly means. Month indicated by numbers at top of panel; population name indicated at right of each row. *Crocosphaera* abundance was not measured with the Influx through the HOT program.

and median cell diameters and carbon quotas for each population (Fig. 3). The hourly diameters for both *Prochlorococcus* and *Synechococcus* varied approximately 2-fold: *Prochlorococcus* diameters ranged from 0.39 to 0.76 μm (median = 0.54 μm) and *Synechococcus* diameters from 0.74 to 1.45 μm (median = 0.98 μm). The diameter of *Crocosphaera* varied around 2.5-fold, spanning 1.82–4.68 μm (median = 2.69 μm). The small eukaryotic phytoplankton population displayed nearly a 5-fold diameter variation, from 0.72 to 3.52 μm (median = 1.80 μm), a range likely reflecting the diverse eukaryotic picoplankton composition captured by SeaFlow (Fig. 3). Hourly carbon quota varied more widely than diameter over the daily cycle, which is expected due to the cubic relationship between volume and radius. Both *Prochlorococcus* and *Synechoccocus* carbon quotas varied around 5-fold, ranging from 14 to 75 fg C cell^{-1} (median = 30 fg C cell^{-1}) and 69 to 390 fg C cell^{-1} (median = 141 fg C cell^{-1}), respectively. The carbon quota of *Crocosphaera* showed about 13-fold variation in carbon quota, ranging from 710 to 8910 fg C cell^{-1} (median = 1950 fg C cell^{-1}). Finally, the small eukaryotic phytoplankton population displayed the greatest variation in carbon quota, ranging approximately 60-fold from 64 to 3870 fg C cell^{-1} (median = 690 fg C cell^{-1}).

To estimate the cellular growth rates (h^{-1}) of each phytoplankton population (Fig. 4), we used the exponential rate of change in hourly mean carbon quota from sunrise to sunset. The cellular growth rates for *Prochlorococcus*, *Synechococcus*, and the small eukaryotic phytoplankton varied approximately 7-fold, while those for *Crocosphaera* varied about 3.2-fold throughout the study period. Specifically, *Prochlorococcus* growth rates ranged from 0.015 to 0.11 h^{-1} (median = 0.045 h^{-1}), *Synechococcus* from 0.010 to 0.084 h^{-1} (median = 0.037 h^{-1}), small eukaryotic phytoplankton from 0.021 to 0.17 h^{-1} (median = 0.076 h^{-1}), and *Crocosphaera* from 0.036 to 0.15 h^{-1} (median = 0.090 h^{-1}). Overall, the median cellular growth rates were significantly different

Table 1. Annual and seasonal abundances of *Prochlorococcus*, *Synechococcus*, small eukaryotes, and *Crocosphaera* populations based on SeaFlow data. Standard deviations (in parentheses) were calculated from daily means. Winter (W): December–February; Spring: March–May; Summer (S): June–August; Fall: September–November. W/S = winter mean/summer mean × 100%. The *p* values indicate the level of significance among seasons (Kruskal–Wallis test, $p < 0.01$).

	Abundance (10^6 cells L^{-1})						
Population	**Annual**	**Winter**	**Spring**	**Summer**	**Fall**	**W/S (%)**	***p***
Prochlorococcus	201	205	185	200	208	102.5	0.11
	(46.1)	(47.9)	(43.2)	(47.2)	(43.4)		
Synechococcus	1.47	1.72*	2.01*	1.25†	1.07†	137.6	1.5×10^{-6}
	(0.9)	(0.99)	(0.952)	(0.768)	(0.633)		
Small eukaryotes	1.74	1.79‡	2.10‡	1.83	1.26†	97.8	2.5×10^{-4}
	(1.30)	(0.85)	(1.13)	(1.72)	(1.03)		
Crocosphaera	0.08	0.010*	0.015*	0.128†	0.127†	12.0	9.5×10^{-17}
	(0.13)	(0.005)	(0.0226)	(0.169)	(0.128)		

*Significant difference from both summer and fall.
†Significant difference ($p < 0.01$) from both winter and spring.
‡Significant difference from fall only based on the Dunn test.

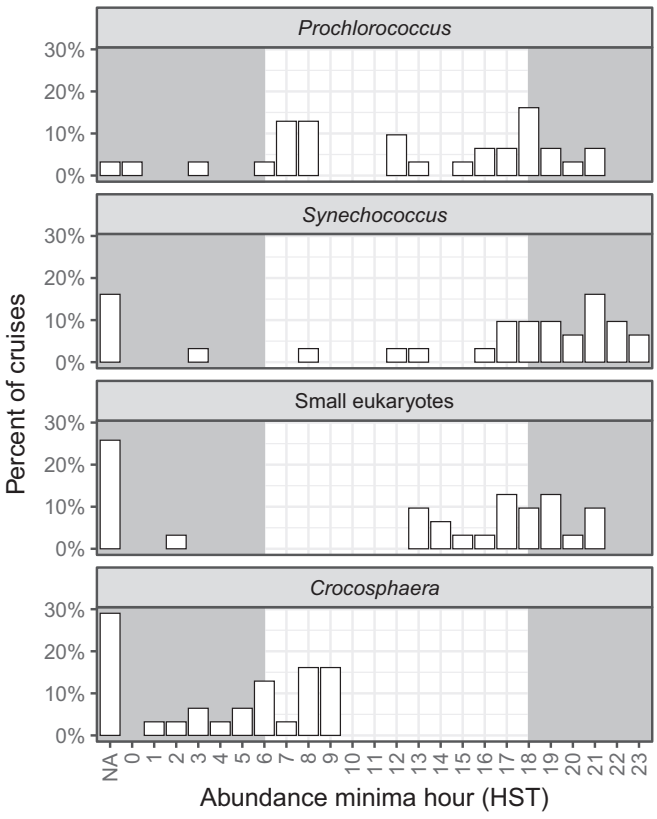

Fig. 2. Percent of cruises (31 total) that displayed an abundance minimum at a given hour of day. NA: cruises for which abundance was not significantly rhythmic ($p \geq 0.01$). Background shading: gray = night, white = day.

among the populations (Kruskal–Wallis rank sum test, $p \leq 2.2 \times 10^{-16}$), except between small eukaryotes and *Crocosphaera* where the difference was not significant (Dunn test, $p = 0.0344$).

Variability at different time scales

We assessed the variability in abundance and cellular growth rate by calculating the fold change at sequential time steps, ranging from hourly to annual scales (Fig. 5). For *Prochlorococcus* and *Synechococcus*, variability in abundance increased from hourly to monthly scales and then decreased from monthly to annual scales. The distribution of hourly variability significantly differed from daily, monthly, and seasonal scales for both populations. Additionally, daily variability was significantly different from seasonal for *Synechococcus* only (Dunn test; $p < 0.01$). In contrast, for both small eukaryotes and *Crocosphaera*, median variability in abundance progressively increased as the time step extended; both hourly and daily variability were significantly lower than seasonal and annual variability (Dunn test; $p < 0.01$). Variability in cellular growth rate did not display significantly differences across time scales for any of the populations (Kruskal–Wallis, $p > 0.01$). It is worth noting that the seasonal variability data for *Crocosphaera* cellular growth rate consisted only of two points.

Carbon biomass and net productivity

Prochlorococcus biomass dominated the total detected biomass, ranging from ~ 5 to 7.5 μg C L^{-1} for most of the year, except during sporadic summer blooms of small eukaryotic phytoplankton. During these blooms, eukaryotic phytoplankton biomass was comparable to that of *Prochlorococcus* (Fig. 6, top panel). *Crocosphaera* biomass contributed between 6.4% and 15.1% of the total biomass during its own blooms, while its contribution was around 1.2% ± 2.1% during nonbloom periods. *Synechococcus* biomass remained consistently low throughout the time series.

At Station ALOHA, the biomass of phytoplankton less than 5 μm as measured by Seaflow made up 18% to 64% of the particulate carbon during cruises without small eukaryote blooms,

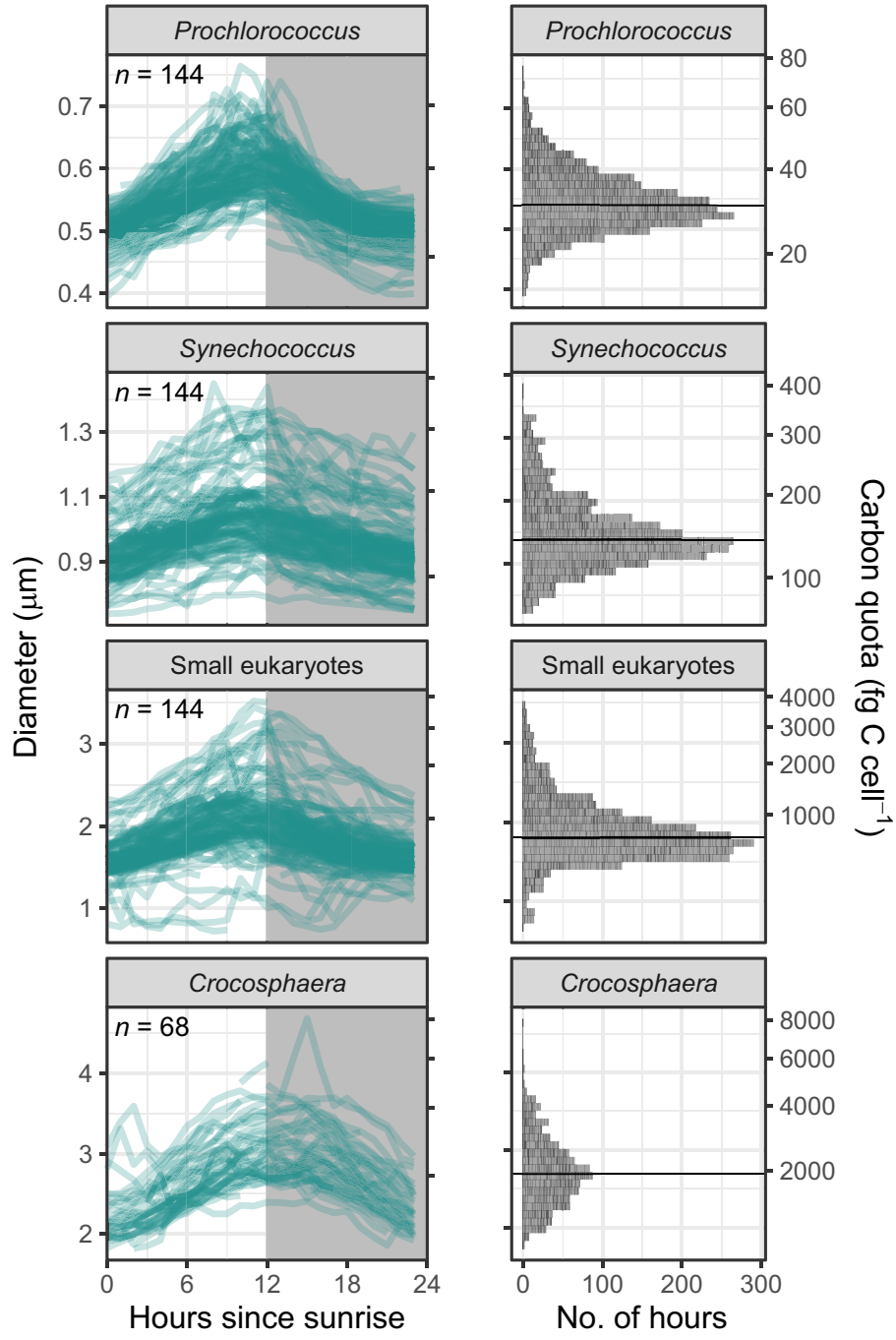

Fig. 3. Estimated diameter (μm, left *y*-axes) and carbon quota (fg C cell^{-1}, right *y*-axes) for *Prochlorococcus*, *Synechococcus*, eukaryotic phytoplankton < 5 μm, and *Crocosphaera* populations. Left panels: each line represents the change in hourly mean cell diameter over the course of a day. White shading indicates day light, gray indicates night time, and *n* is the number of days included. Right panels: distribution of hourly mean cell diameter or carbon quota. Black horizontal lines indicate median values of the distribution for each population.

and 31% to 67% during bloom occurrences (Fig. 6, top panel). Net carbon productivities (μg C L^{-1} d^{-1}) for the four phytoplankton populations were estimated by scaling their cellular growth rates to the mean abundance observed at sunrise. These values were generally similar to or lower than estimates obtained through the ^{14}C-based method, except during three of the four summer eukaryote blooms (Fig. 6, bottom panel). During these transient blooms, net carbon productivity estimated by SeaFlow ranged from 138% to 300% of the ^{14}C-based estimates.

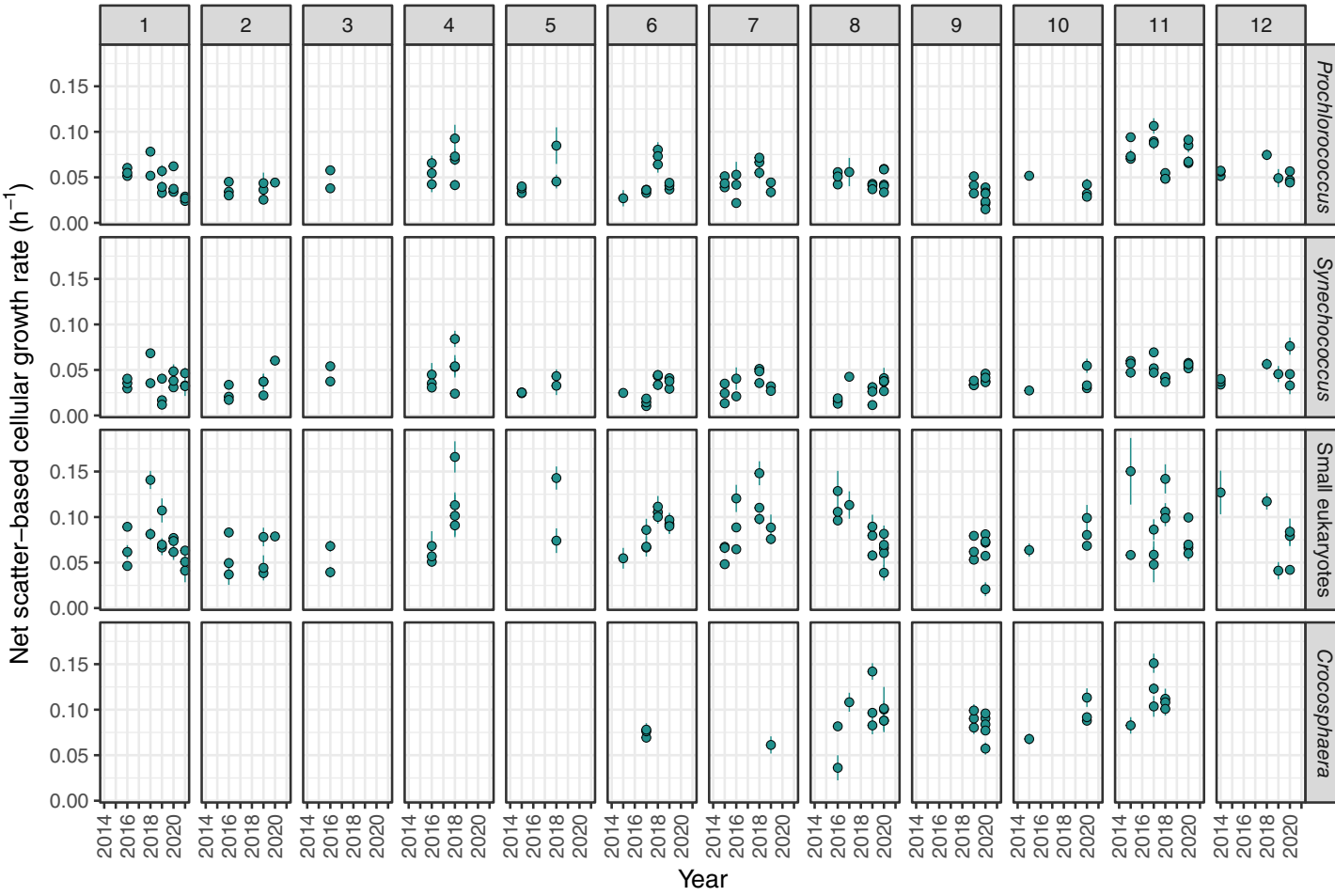

Fig. 4. Cellular growth rates (h^{-1}) for *Prochlorococcus*, *Synechococcus*, eukaryotic phytoplankton < 5 μm, and *Crocosphaera* populations. Rates were derived from changes in carbon cell content derived from forward light scatter during daylight hours. Vertical bars indicate residual standard error.

Discussion

Seasonal and diel variability

Here, we deployed SeaFlow, a continuous shipboard flow cytometer, on 42 multiday cruises in the NPSG to assess temporal variability in the surface mixed layer of cell abundance, biomass, cellular growth rates, and primary productivity for *Prochlorococcus*, *Synechococcus*, *Crocosphaera*, and eukaryotic phytoplankton less than 5 μm in diameter. The SeaFlow data were consistent with time-series data from the Hawaii Ocean Time-series (HOT) program, aligning well on both seasonal and annual scales (Fig. 1; Supporting Information Fig. S3). For example, SeaFlow observations agreed with previous results by Campbell et al. (1997) showing surface abundance peaks of small eukaryotic phytoplankton and *Crocosphaera* in the summer, *Synechococcus* in the winter, and a lack of seasonality in *Prochlorococcus* abundances (Table 1).

At the diel scale, cell abundances, cell size, and carbon quotas of phytoplankton populations smaller than 5 μm in equivalent spherical diameter aligned closely with the day/night cycle. Observations from *Prochlorococcus*, *Synechococcus*, and small eukaryotic phytoplankton daily time series showed cell abundance minima typically occurring toward dusk and early evening (16:00–22:00), whereas *Crocosphaera* minima occurred near or after dawn (04:00–10:00) (Fig. 2). Furthermore, cell diameter and carbon quota displayed a high degree of synchronization (Fig. 3; Supporting Information Fig. S4), with *Prochlorococcus*, *Synechococcus*, and small eukaryotic phytoplankton reaching carbon quota maxima during the hours around dusk, while *Crocosphaera* showed carbon quota maxima late in the evening, diverging from its cell abundance minima observed at dawn. The observed patterns in cell abundance minima and carbon quota maxima are consistent with the anticipated timing of cell division within these phytoplankton populations, suggesting the increase in cell abundance signals the onset of cell division processes (Jacquet et al. 2001; Binder and DuRand 2002; Wilson et al. 2017). The dynamics of *Crocosphaera* stands apart, as this species experiences a significant reduction in carbon quota during the energy-intensive N_2 fixation at night followed by cell division in the morning, indicating a distinct metabolic and cell division rhythm (Dron et al. 2012; Wilson

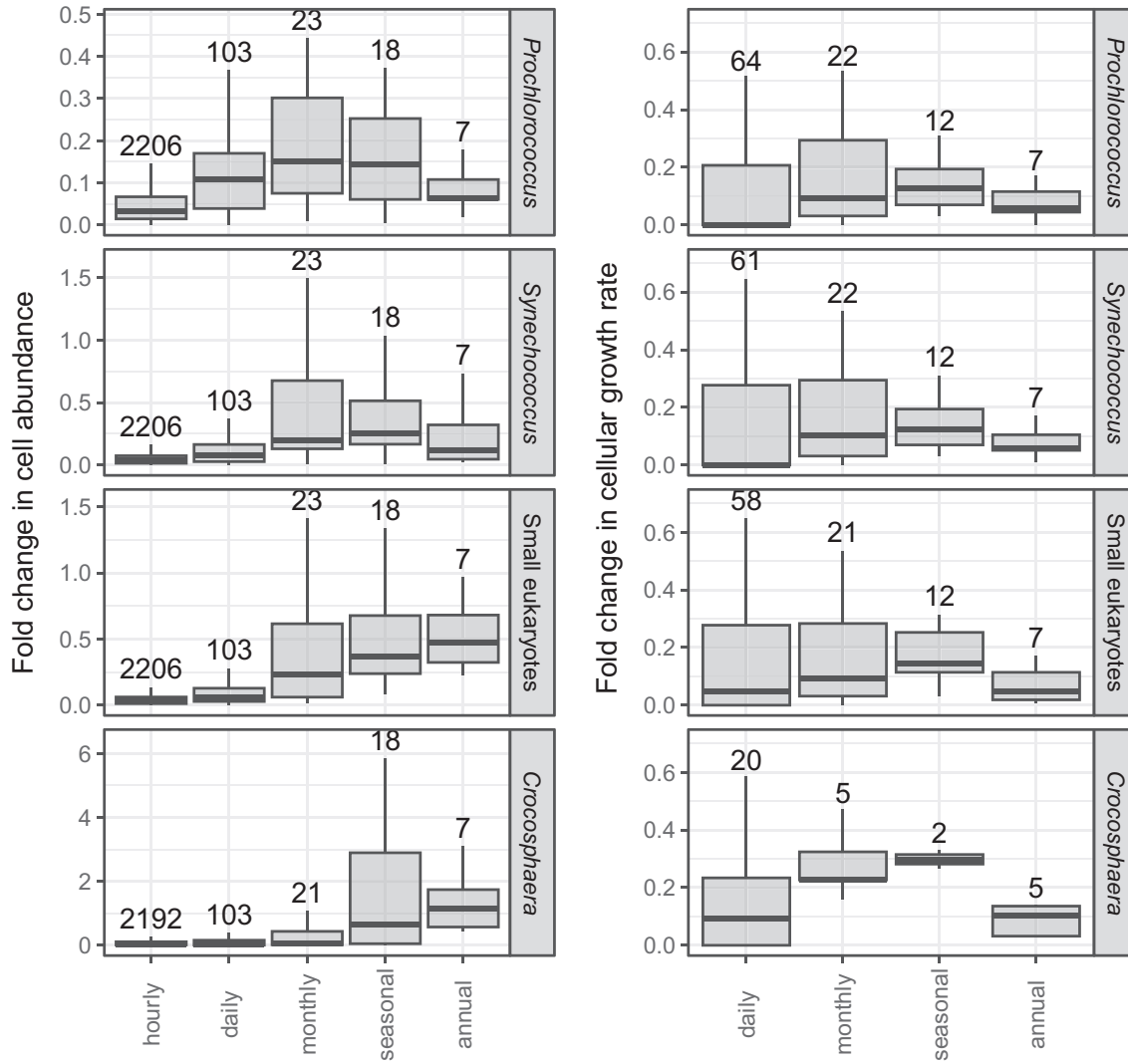

Fig. 5. Variability in abundance (left) and cellular growth rate (right) calculated by the fold change in sequential time steps at different time scales: hourly (abundance only), daily, monthly, seasonal, and annual. The central line is the median, the edges of the box denote 25th and 75th quantiles, and the whiskers denote the range, excluding outliers that are more than 1.5 × the inter-quantile distance below or above the 25th and 75th quantiles, respectively. Numbers indicate the number of data points for each box. Note that the *y*-axis limits in the left panel vary by population.

et al. 2017). Contrary to previous flow cytometry studies in the Equatorial Pacific (4°S–5°N), which reported *Synechococcus* dividing first in the afternoon, followed by *Prochlorococcus* and then picoeukaryotes (Vaulot and Marie 1999; Binder and DuRand 2002), our results suggest a different timing. Our abundance data show *Prochlorococcus* dividing on average before *Synechococcus*, while our carbon quota maxima indicate *Synechococcus* likely dividing before *Prochlorococus*. Moreover, our results for small eukaryotes diverge from previous studies (Vaulot and Marie 1999); instead of dividing in the middle of the night, we observed division primarily between 15:00 and 21:00. These differences may be attributed to varying habitat conditions, as earlier studies were conducted in Equatorial Pacific regions with higher abundances of *Synechococcus* and small eukaryotic phytoplankton compared to Station ALOHA. Our findings align more closely with those from the South China Sea (Li et al. 2022a), underscoring the influence of strain and environmental conditions on the timing of cell division (Jacquet et al. 2001), which can exhibit considerable variation (Binder and DuRand 2002). A significant fraction of the *Prochlorococcus* time series displayed abundance minima in the morning rather than the commonly observed pattern around dusk. This deviation might stem from physical processes such as advection or could be an artifact resulting from the smallest *Prochlorococcus* cells evading detection. However, there have been prior reports of *Prochlorococcus* abundances increasing in the morning, which could be attributed to cells already in G2 phase at the start of the day that subsequently divide, as observed in ultradian growth cycles (Shalapyonok et al. 1998; Ribalet et al. 2015).

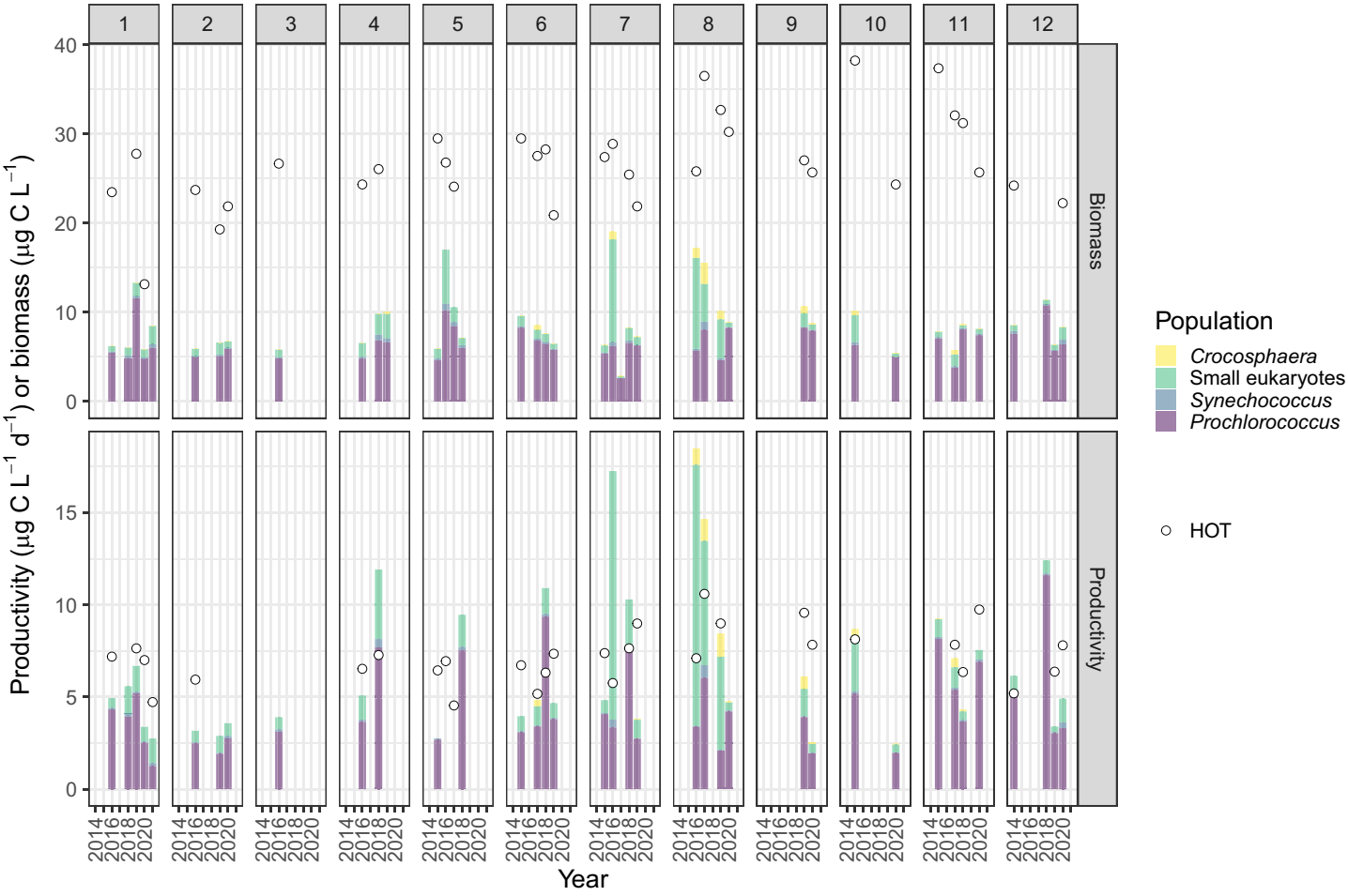

Fig. 6. Mean biomass (upper panels) and productivity (lower panels) for each of the four picophytoplankton groups over different months (as indicated by numbers on top of upper panels) and years. Purple: *Prochlorococcus*; blue: *Synechococcus*; green: eukaryotic phytoplankton ≤ 5 μm in diameter; yellow: *Crocosphaera*. White circles in upper panels: total particulate carbon from Hawaii Ocean Time-series (HOT) data. White circles in lower panels: ^{14}C-based primary productivity for HOT data.

The synchrony of abundance minima with the expected timing of cell division indicated a temporal offset between cell division and mortality processes (e.g., Binder and DuRand 2002; Ribalet et al. 2015). Sources of phytoplankton mortality at Station ALOHA are best understood for *Prochlorococcus*. In surface waters, grazing by heterotrophic and mixotrophic protists emerges as the dominant mortality factor in this population (Calbet and Landry 1999; Connell et al. 2020), whereas viral lysis accounts for less than 5% of the observed daily mortality (Mruwat et al. 2021). Heterotrophic protists primarily feed at night, while mixotrophic protists are active throughout the day (Connell et al. 2020). Due to these feeding behaviors, *Prochlorococcus* reaches a peak in abundance after midnight before being reduced by nocturnal grazing by the heterotrophic grazers. Similar ecological interactions likely occur with *Synechococcus* and the small eukaryotic phytoplankton, making it crucial to understand the grazing habits of these protists for a comprehensive understanding of marine food web dynamics at Station ALOHA.

At the seasonal scale, we observed recurrent blooms of small eukaryotic phytoplankton and *Crocosphaera* during the summer months (Fig. 1). These blooms, defined as cell abundances two standard deviations above the mean, were congruous with previous observations for *Crocosphaera* (Campbell et al. 1997; Church et al. 2009) and puzzling for small eukaryotic phytoplankton; while eukaryotic blooms were consistently detected by SeaFlow, the HOT program's flow cytometer measured among the lowest abundances of the series (Supporting Information Fig. S6). This discrepancy could stem from the differences in instrumentation and sampling protocols. The HOT program employs a conventional flow cytometer to analyze fixed and cryopreserved cells collected from Niskin bottles, a process that preserves picocyanobacteria well but can eventually lead to cell loss in fragile species, especially dinoflagellates and cryptophytes (Vaulot et al. 1989; Eschbach et al. 2001; Liu et al. 2022). On the other hand, SeaFlow measures live cells directly from underway seawater and uses virtual core technology to optimize optical cell properties (Swalwell et al. 2011) While this approach

avoids the potential cell loss, it introduces uncertainties in calibration that must be considered in data interpretation (Ribalet et al. 2019). These blooms have been consistently observed over multiple years and with different SeaFlow instruments, suggesting that they are real biological events. They also align with known phytoplankton dynamics at Station ALOHA during summer months, including the high abundances of small phytoplankton like prymnesiophytes, autotrophic flagellates, diatoms, and autotrophic dinoflagellates (Brzezinski et al. 1998; Scharek et al. 1999; Calbet et al. 2001; Pasulka et al. 2013). However, phytoplankton enumeration in these prior studies primarily relied on aldehyde-preserved samples, settling chambers, or light microscopy which might not detect cells smaller than 5 μm in diameter and therefore do not offer a direct comparison for our observations, particularly regarding the community composition of smaller phytoplankton in the NPSG during summer. Material collected from traps at depth during summer contained small eukaryotic phytoplankton such as small centric diatoms and other stramenopile lineages, green algae, and haptophytes (Poff et al. 2021), which suggests that these small blooms may play a significant role in the pulse of carbon export observed in summer at Station ALOHA (Karl et al. 1996, 2021). Nonetheless, the lack of detection by the HOT program's flow cytometer could point toward biases in the SeaFlow methodology. If these blooms are authentic biological events, the nitrogen source required for fueling these blooms remains unclear. Nutrient supply from depth to surface waters at Station ALOHA is limited, particularly in the summer months due to increased stratification. Previous observations suggest that nitrogen for summer blooms is usually supplied through nitrogen fixation (Winn et al. 1995; Dore et al. 2002) by species such as the cyanobacteria *Trichodesmium*, *Crocosphaera*, and UCYN-A (Church et al. 2009; Pasulka et al. 2013; Karl and Church 2014) or by nitrogen-fixing cyanobacterial symbionts associated with diatoms such as *Hemialus hauckii* (Brzezinski et al. 1998; Scharek et al. 1999; Villareal et al. 2012; Pasulka et al. 2013; White et al. 2015). Although the observed eukaryotic phytoplankton blooms frequently coincided with *Crocosphaera* blooms, no direct correlation between their abundances has been established (Supporting Information Fig. S8). Given these considerations, it is difficult to conclusively categorize these blooms as either authentic biological events or instrument artifacts based solely on the available information. Additional studies using multiple, complementary methodologies are warranted to draw more conclusive interpretations.

We assessed the variations in cell abundance of phytoplankton populations over different time scales by calculating the fold change from one time period to the next, revealing distinct patterns of abundance variability (Fig. 5). *Prochlorococcus* and *Synechococcus* showed the highest variability at monthly intervals, whereas small eukaryotic phytoplankton and *Crocosphaera* exhibited increased variability on an annual scale. These findings align with variability in surface primary production at Station ALOHA, consisting of 64% sub-seasonal, 11% seasonal, and 23% interannual components, while variability in Chl *a* is 72% sub-seasonal, 17% seasonal, and 11% interannual (Karl et al. 2021). Sub-seasonal variability is likely driven by the small picocyanobacteria *Prochlorococcus* and *Synechococcus* whereas the seasonal to interannual variability is partially driven by the relatively larger phytoplankton, such as small eukaryotic phytoplankton and *Crocosphaera*, possibly as a result of episodic summer blooms. This difference in temporal dynamics among these populations suggests that phytoplankton <5 μm respond differently to environmental changes, operating on different time scales.

Biomass and primary productivity

In addition to measuring cell abundance, SeaFlow offers a continuous readout of each cell's forward light scatter. We calibrated this light scatter to infer an equivalent spherical diameter for the cells (Ribalet et al. 2019), which was then used for estimating carbon quota via a cell volume-to-carbon conversion factor for small phytoplankton (Menden-Deuer and Lessard 2000). While our approach has inherent uncertainties primarily due to variations in the refractive indices among species (Lehmuskero et al. 2018) and differences in cellular composition (Henderikx-Freitas et al. 2022), the similarity between our estimates and those obtained using more conventional methods provides support for the use of light scatter data for carbon quota estimation. Specifically, our median carbon quota estimate for *Prochlorococcus* was 30 fg C cell^{-1}, aligning closely with the 26 fg C cell^{-1} estimate derived from size-fractionated particulate carbon measurements at Station ALOHA (Casey et al. 2019). For *Synechococcus*, our median carbon quota was 150 fg C cell^{-1}, consistent with estimates from isolates cultured under similar temperatures ($\sim$ 180 fg C cell^{-1}; fu : pico). Estimates for *Crocosphaera* ranged between 0.7 and 8.9 pg C cell^{-1}, falling within the 1.2 – 10.1 pg C cell^{-1} range observed for small and large *Crocosphaera* cells (Wilson et al. 2017). Regarding eukaryotic phytoplankton, we noted year-to-year variations in carbon quotas, with higher cell quotas observed in August 2016 (1.42 – 2.70 pg C cell^{-1} interquartile range, equivalent to 2.39–3.06 μm in diameter) compared to August 2019 (0.92 – 1.67 pg C cell^{-1} interquartile range, equivalent to 2.02–2.54 μm diameter) (Supporting Information Fig. S6). These estimates are in line with known carbon quotas for eukaryotic isolates, such as the open-ocean green algae *Chloropicon* and *Micromonas* species (0.45 – 0.75 pg C cell^{-1}), and the model diatom *Thalassiosira pseudonana* (0.6 – 1.2 pg C cell^{-1}, depending on light intensity and nutrient availability) (Shi et al. 2015; Liefer et al. 2019; Ebenezer et al. 2022). Our estimates of carbon quotas across various phytoplankton species are consistent with previous studies and support the use of light scatter data for such estimates despite inherent uncertainties.

Carbon biomass was estimated from median carbon quotas and cell abundances for each phytoplankton population. Generally, *Prochlorococcus* dominated the small phytoplankton biomass, accounting for 60%–95% of the biomass with

concentrations ranging from 2.6 to 11.6 μg C L^{-1}. Small eukaryotes were the second highest contributor, with biomass concentrations between 0.15 and 11.5 μg C L^{-1}. A previous study using epifluorescent microscopy reported that eukaryotic phytoplankton with equivalent spherical diameter of 2–5 μm constituted approximately 20% of the autotrophic biomass unless large nitrogen-fixing cyanobacteria (> 40 μm) like *Trichodesmium* were abundant (Pasulka et al. 2013). During the summer when eukaryote abundance spiked, *Prochlorococcus* and eukaryotes contributed 32–52% and 27–60% of the total small phytoplankton biomass, respectively. The combined biomass peaked at 19 μg C L^{-1} in 2016; while C : Chl *a* is highly variable and depends on season and community composition (Campbell et al. 1994) this biomass would be equivalent to 0.14 μg Chl *a* L^{-1} based on a C : Chl *a* ratio of 128 : 1 ± 48 (Campbell et al. 1994). This is 2–3 times the Chl *a* concentrations measured by HOT via HPLC during these cruises (~0.05 – 0.08 μg Chl *a* L^{-1}) and is greater than the chlorophyll concentration range measured by HPLC at Station ALOHA in August throughout the HOT program (0.05 – 0.012 μg Chl *a* L^{-1}). Satellite-based chlorophyll data during the timing of these blooms were unavailable due to cloudy conditions at Station ALOHA.

The rate of change of the mean hourly carbon quota for each phytoplankton population during daylight was used to estimate cellular growth rates. Across the different phytoplankton populations, no significant variations in growth rates were observed across different time scales (Fig. 5), and contrary to our expectations no seasonal pattern in growth rates was found. Median cellular growth rates for the larger cells including small eukaryotic phytoplankton and *Crocosphaera* were about twice as high as rates for the smaller cells, *Prochlorococcus* and *Synechococcus*. This disparity in growth rates across different cell sizes aligns with a unimodal quadratic relationship between cell diameter and growth rate, where maximum growth rates occur at 2.8 μm (measured by ^{14}C uptake) and 5.4 μm (measured by dilution method). These peak sizes encompass the larger cells detected by SeaFlow (Chen and Liu 2010). The median growth rate for *Prochlorococcus* was 0.045 h^{-1}, in good agreement with rates of 0.05 – 0.1 h^{-1} estimated by ^{14}C assimilation (Casey et al. 2019). For *Synechococcus*, the median growth rate was 0.037 h^{-1}, consistent with culture-based measurements (Fu et al. 2007), and about 20% slower than *Prochlorococcus*. Small eukaryotic phytoplankton displayed high median growth rates, at 0.076 h^{-1} (Fig. 4). *Crocosphaera* could only be evaluated for growth rates from June to December when cell abundances were high enough. During this period, *Crocosphaera* displayed the highest median growth rates of 0.090 h^{-1}. These elevated growth rates may reflect high daytime carbon storage needed to meet the energy demands for N_2 fixation at night (Dron et al. 2012; Masuda et al. 2023). Assuming a 30% respiratory loss of fixed carbon (Masuda et al. 2023), the cumulative daylight growth rates for *Crocosphaera* (1.08 d^{-1}) would yield division rates of 0.76 d^{-1}, higher than previous estimates near Station ALOHA (0.6 d^{-1}, Wilson et al. 2017). Although cellular growth is essential for increasing cell abundance, growth rates were not directly correlated to abundance ($R^2 < 0.0075$, $p > 0.40$) or to daily fold changes in abundance in this study ($R^2 < 0.02$, $p > 0.14$; Supporting Information Fig. S5) and further emphasize the importance of loss processes such as mortality in controlling phytoplankton standing stocks at Station ALOHA.

Mean net productivity for each cruise was calculated from cellular growth rates and population-specific abundance. Throughout much of the SeaFlow time series, measured productivity was lower than that assessed by the HOT program. This discrepancy is attributable to differences in both estimation methods and the range of phytoplankton populations sampled, with SeaFlow measuring only cells smaller than 5 μm in diameter. During winter, SeaFlow-based productivity estimates ranged from 2.5 to 5 μg C L^{-1} d^{-1}, approximately 50–60% of the surface ^{14}C-based rates (5.2 – 7.6 μg C L^{-1} d^{-1}) measured by the HOT program. This was primarily driven by *Prochlorococcus* and is consistent with cell-sorted ^{14}C productivity measurements (Rii et al. 2016). Remarkably, despite the inherent uncertainties in both the cytometry-based SeaFlow and the radiocarbon-based HOT methods, they produce estimates that are in a reasonable range of one another. This agreement is especially noteworthy given the fundamentally different principles upon which these approaches are based. SeaFlow's ability to produce productivity rates that closely align with the more established ^{14}C method lends credence to the robustness of both methodologies, and reinforces the value of employing multiple, complementary approaches for a more comprehensive understanding of marine productivity.

High SeaFlow-based productivity was observed during the cryptic summer blooms of small eukaryotic phytoplankton. During these events, estimated productivity doubled the ^{14}C-based rates, reaching 17 – 20 μg C L^{-1} d^{-1} (Fig. 6). One possibility for this discrepancy is that the SeaFlow methodology could overestimate the abundance of eukaryotic phytoplankton abundance during the summer, thereby affecting productivity estimates. Alternatively, these blooms could be genuine biological events, potentially exposing issues such as bottle effects during ^{14}C incubations. One intriguing possibility that requires further exploration is that the bloom organisms may be mixotrophic, fulfilling C and N requirements via phagotrophy while retaining the ability to carry out photosynthesis (Edwards 2019; Lambert et al. 2022; Li et al. 2022b), which are more common under N-limiting conditions (Mitra et al. 2016; Edwards et al. 2023). While bottle effects may be a factor, they do not account for the nitrogen requirements of these eukaryotic cells. Our estimates suggest *Crocosphaera* could fix 1.45 – 15.4 nmol N L^{-1} d^{-1}, based on a N_2 fixation

rate of $18.3 \pm 3.75 \times 10^{-6}$ nmol Ncell^{-1} d^{-1} (Wilson et al. 2017). Although sufficient to meet its own requirements for primary productivity ($0.037 - 1.79$ μg C L^{-1} d^{-1}), this rate would not provide enough nitrogen for the surrounding phytoplankton. Other nitrogen-fixing species such as *Trichodesmium* and diatom–diazotroph associations, known to be present year-round at Station ALOHA (White et al. 2007; Church et al. 2009), could contribute to eukaryotic growth. Alternatively, these eukaryotic blooms might satisfy much of their nitrogen needs via phagotrophy, creating a shift in carbon cycling within the system (Ward and Follows 2016). Further research would be needed to validate the role of mixotrophy at Station ALOHA during late summer.

Conclusion

The deployment of SeaFlow in the NPSG on 42 multiday cruises has enabled analysis of the temporal variability of phytoplankton populations at cellular levels, which is central to our understanding of marine ecosystems and biogeochemical cycles. Notably, our observations of cell abundance, biomass, and primary productivity align well with existing time-series data from the HOT program, thereby validating the utility of the technology. SeaFlow's continuous data revealed complex patterns in both diel and seasonal scales, with the timing of phytoplankton cell division and mortality processes often aligned with day/night cycles. Variability in abundance for *Prochlorococcus* and *Synechococcus* peaked at monthly scales while variability for small eukaryotic phytoplankton and *Crocosphaera* peaked at seasonal to annual scales. This interannual variability was likely due to puzzling recurrent blooms of small eukaryotic phytoplankton and *Crocosphaera* detected by SeaFlow in the summer months that went unmeasured by the HOT program, opening the door to questions about methodology, instrumentation, and the very nature of these biological events. While our observations align with established knowledge about seasonal nitrogen fixation and phytoplankton dynamics, the source of nitrogen fueling these summer blooms remains an area for future exploration.

Data availability statement

The data that support the findings of this study are openly available in Zenodo at http://doi.org/10.5281/zenodo.7154076.

References

Barone, B., A. R. Coenen, S. J. Beckett, D. J. McGillicuddy Jr., J. S. Weitz, and D. M. Karl. 2019*a*. The ecological and biogeochemical state of the North Pacific Subtropical Gyre is linked to sea surface height. J. Mar. Res. **77**: 215–245. doi:10.1357/002224019828474241

Barone, B., D. Nicholson, S. Ferrón, E. Firing, and D. Karl. 2019*b*. The estimation of gross oxygen production and community respiration from autonomous time-series measurements in the oligotrophic ocean. Limnol. Oceanogr.: Methods **17**: 650–664. doi:10.1002/lom3.10340

Barone, B., and others. 2022. Biogeochemical dynamics in adjacent mesoscale eddies of opposite polarity. Global Biogeochem. Cycles **36**: e2021GB007115. doi:10.1029/2021GB007115

Binder, B. J., and M. D. DuRand. 2002. Diel cycles in surface waters of the equatorial Pacific. Deep-Sea Res. II Top. Stud. Oceonogr. **49**: 2601–2617. doi:10.1016/S0967-0645(02)00050-4

Brzezinski, M. A., T. A. Villareal, and F. Lipschultz. 1998. Silica production and the contribution of diatoms to new and primary production in the central North Pacific. Mar. Ecol. Prog. Ser. **167**: 89–104. doi:10.3354/meps167089

Calbet, A., and M. R. Landry. 1999. Mesozooplankton influences on the microbial food web: Direct and indirect trophic interactions in the oligotrophic open ocean. Limnol. Oceanogr. **44**: 1370–1380. doi:10.4319/lo.1999.44.6.1370

Calbet, A., M. R. Landry, and S. Nunnery. 2001. Bacteria–flagellate interactions in the microbial food web of the oligotrophic subtropical North Pacific. Aquat. Microb. Ecol. **23**: 283–292. doi:10.3354/ame023283

Campbell, L., H. A. Nolla, and D. Vaulot. 1994. The importance of *Prochlorococcus* to community structure in the central North Pacific Ocean. Limnol. Oceanogr. **39**: 954–961. doi:10.4319/lo.1994.39.4.0954

Campbell, L., H. Liu, H. A. Nolla, and D. Vaulot. 1997. Annual variability of phytoplankton and bacteria in the subtropical North Pacific Ocean at station ALOHA during the 1991–1994 ENSO event. Deep Sea Res. I Oceanogr. Res. Pap. **44**: 167–192. doi:10.1016/S0967-0637(96)00102-1

Casey, J. R., K. M. Björkman, S. Ferrón, and D. M. Karl. 2019. Size dependence of metabolism within marine picoplankton populations. Limnol. Oceanogr. **64**: 1819–1827. doi:10.1002/lno.11153

Chen, B., and H. Liu. 2010. Relationships between phytoplankton growth and cell size in surface oceans: Interactive effects of temperature, nutrients, and grazing. Limnol. Oceanogr. **55**: 965–972. doi:10.4319/lo.2010.55.3.0965

Church, M. J., C. Mahaffey, R. M. Letelier, R. Lukas, J. P. Zehr, and D. M. Karl. 2009. Physical forcing of nitrogen fixation and diazotroph community structure in the North Pacific subtropical gyre. Global Biogeochem. Cycl. **23**: GB2020. doi:10.1029/2008GB003418

Connell, P. E., F. Ribalet, E. V. Armbrust, A. White, and D. A. Caron. 2020. Diel oscillations in the feeding activity of heterotrophic and mixotrophic nanoplankton in the North Pacific Subtropical Gyre. Aquat. Microb. Ecol. **85**: 167–181. doi:10.3354/ame01950

Dore, J. E., J. R. Brum, L. M. Tupas, and D. M. Karl. 2002. Seasonal and interannual variability in sources of nitrogen supporting export in the oligotrophic subtropical North Pacific Ocean. Limnol. Oceanogr. **47**: 1595–1607. doi:10.4319/lo.2002.47.6.1595

Dore, J. E., R. M. Letelier, M. J. Church, R. Lukas, and D. M. Karl. 2008. Summer phytoplankton blooms in the oligotrophic North Pacific Subtropical Gyre: Historical perspective and recent observations. Prog. Oceanogr. **76**: 2–38. doi:10.1016/j.pocean.2007.10.002

Dron, A., S. Rabouille, P. Claquin, B. L. Roy, A. Talec, and A. Sciandra. 2012. Light–dark (12:12) cycle of carbon and nitrogen metabolism in *Crocosphaera watsonii* WH8501: Relation to the cell cycle. Environ. Microbiol. **14**: 967–981. doi:10.1111/j.1462-2920.2011.02675.x

Dugenne, M., and others. 2023. Nitrogen fixation in mesoscale eddies of the North Pacific Subtropical Gyre: Patterns and mechanisms. Global Biogeochem. Cycles **37**: e2022GB007386. doi:10.1029/2022GB007386

Ebenezer, V., Y. Hu, O. Carnicer, A. J. Irwin, M. J. Follows, and Z. V. Finkel. 2022. Elemental and macromolecular composition of the marine Chloropicophyceae, a major group of oceanic photosynthetic picoeukaryotes. Limnol. Oceanogr. **67**: 540–551. doi:10.1002/lno.12013

Edwards, K. F. 2019. Mixotrophy in nanoflagellates across environmental gradients in the ocean. Proc. Natl. Acad. Sci. USA **116**: 6211–6220. doi:10.1073/pnas.1814860116

Edwards, K. F., Q. Li, K. A. McBeain, C. R. Schvarcz, and G. F. Steward. 2023. Trophic strategies explain the ocean niches of small eukaryotic phytoplankton. Proc. R. Soc. B Biol. Sci. **290**: 20222021. doi:10.1098/rspb.2022.2021

Eschbach, E., M. Reckermann, U. John, and L. K. Medlin. 2001. Optimization of preservation methods provides insights into photosynthetic picoeukaryotes in lakes. Cytometry **44**: 126–132. doi:10.1002/1097-0320(20010601)44:2<126::AID-CYTO1091>3.0.CO;2-N

Ferrón, S., S. T. Wilson, S. Martínez-García, P. D. Quay, and D. M. Karl. 2015. Metabolic balance in the mixed layer of the oligotrophic North Pacific Ocean from diel changes in O_2/Ar saturation ratios. Geophys. Res. Lett. **42**: 3421–3430. doi:10.1002/2015GL063555

Fong, A. A., D. M. Karl, R. Lukas, R. M. Letelier, J. P. Zehr, and M. J. Church. 2008. Nitrogen fixation in an anticyclonic eddy in the oligotrophic North Pacific Ocean. ISME J. **2**: 663–676. doi:10.1038/ismej.2008.22

Fu, F.-X., M. E. Warner, Y. Zhang, Y. Feng, and D. A. Hutchins. 2007. Effects of increased temperature and CO_2 on photosynthesis, growth, and elemental ratios in marine *Synechococcus* and *Prochlorococcus* (Cyanobacteria). J. Phycol. **43**: 485–496. doi:10.1111/j.1529-8817.2007.00355.x

Henderikx-Freitas, F., M. Dugenne, F. Ribalet, A. Hynes, B. Barone, D. M. Karl, and A. E. White. 2020. Diel variability of bulk optical properties associated with the growth and division of small phytoplankton in the North Pacific Subtropical Gyre. Appl. Optics **59**: 6702–6716. doi:10.1364/AO.394123

Henderikx-Freitas, F., J. G. Allen, B. M. Lansdorp, and A. E. White. 2022. Diel variations in the estimated refractive index of bulk oceanic particles. Opt. Express **30**: 44141–44159. doi:10.1364/OE.469565

Jacquet, S., F. Partensky, J.-F. Lennon, and D. Vaulot. 2001. Diel patterns of growth and division in marine picoplankton in culture. J. Phycol. **37**: 357–369. doi:10.1046/j.1529-8817.2001.037003357.x

Karl, D. M., J. R. Christian, J. E. Dore, D. V. Hebel, R. M. Letelier, L. M. Tupas, and C. D. Winn. 1996. Seasonal and interannual variability in primary production and particle flux at Station ALOHA. Deep-Sea Res. II Top. Stud. Ocenogr. **43**: 539–568. doi:10.1016/0967-0645(96)00002-1

Karl, D. M., and R. Lukas. 1996. The Hawaii Ocean Time-series (HOT) program: Background, rationale and field implementation. Deep-Sea Res. II Top. Stud. Oceanogr. **43**: 129–156. doi:10.1016/0967-0645(96)00005-7

Karl, D. M., and M. J. Church. 2014. Microbial oceanography and the Hawaii Ocean Time-series programme. Nat. Rev. Microbiol. **12**: 699–701. doi:10.1038/nrmicro3333

Karl, D. M., R. M. Letelier, R. R. Bidigare, K. M. Björkman, M. J. Church, J. E. Dore, and A. E. White. 2021. Seasonal-to-decadal scale variability in primary production and particulate matter export at Station ALOHA. Prog. Oceanogr. **195**: 102563. doi:10.1016/j.pocean.2021.102563

Karl, D. M., K. M. Björkman, M. J. Church, L. A. Fujieki, E. M. Grabowski, and R. M. Letelier. 2022. Temporal dynamics of total microbial biomass and particulate detritus at Station ALOHA. Prog. Oceanogr. **205**: 102803. doi:10.1016/j.pocean.2022.102803

Lambert, B. S., R. D. Groussman, M. J. Schatz, S. N. Coesel, B. P. Durham, A. J. Alverson, A. E. White, and E. V. Armbrust. 2022. The dynamic trophic architecture of open-ocean protist communities revealed through machine-guided metatranscriptomics. Proc. Natl. Acad. Sci. USA **119**: e2100916119. doi:10.1073/pnas.2100916119

Lehmuskero, A., M. Skogen Chauton, and T. Boström. 2018. Light and photosynthetic microalgae: A review of cellular- and molecular-scale optical processes. Prog. Oceanogr. **168**: 43–56. doi:10.1016/j.pocean.2018.09.002

Letelier, R. M., J. E. Dore, C. D. Winn, and D. M. Karl. 1996. Seasonal and interannual variations in photosynthetic carbon assimilation at Station ALOHA. Deep-Sea Res. II Top. Stud. Oceanogr. **43**: 467–490. doi:10.1016/0967-0645(96)00006-9

Letelier, R. M., and D. M. Karl. 1996. Role of *Trichodesmium* spp. in the productivity of the subtropical North Pacific Ocean. Mar. Ecol. Prog. Ser. **133**: 263–273. doi:10.3354/meps133263

Li, C., K.-P. Chiang, E. A. Laws, X. Liu, J. Chen, Y. Huang, B. Chen, A.-Y. Tsai, and B. Huang. 2022*a*. Quasi-antiphase diel patterns of abundance and cell size/biomass of

picophytoplankton in the oligotrophic ocean. Geophys. Res. Lett. **49**: e2022GL097753. doi:10.1029/2022GL097753

Li, Q., K. F. Edwards, C. R. Schvarcz, and G. F. Steward. 2022*b*. Broad phylogenetic and functional diversity among mixotrophic consumers of *Prochlorococcus*. ISME J. **16**: 1557–1569. doi:10.1038/s41396-022-01204-z

Liefer, J. D., and others. 2019. The macromolecular basis of phytoplankton C:N:P under nitrogen starvation. Front. Microbiol. **10**: 1–16. doi:10.3389/fmicb.2019.00763

Liu, C., J. L. M. Zhang, F. Wu, M. Ren, J. Yang, Q. Wu, and X. Shia. 2022. Optimization of preservation methods provides insights into photosynthetic picoeukaryotes in lakes. Microbiol. Spect. **10**: 1–12. doi:10.1128/spectrum.02557-21

Masuda, T., G. Bernát, M. Bečková, E. Kotabová, E. Lawrenz, M. Lukeš, J. Komenda, and O. Prášil. 2018. Diel regulation of photosynthetic activity in the oceanic unicellular diazotrophic cyanobacterium *Crocosphaera watsonii* WH8501. Environ. Microbiol. **20**: 546–560. doi:10.1111/1462-2920.13963

Masuda, T., and others. 2023. The balance between photosynthesis and respiration explains the niche differentiation between *Crocosphaera* and *Cyanothece*. Comput. Struct. Biotechnol. J. **21**: 58–65. doi:10.1016/j.csbj.2022.11.029

Menden-Deuer, S., and E. J. Lessard. 2000. Carbon to volume relationships for dinoflagellates, diatoms, and other protist plankton. Limnol. Oceanogr. **45**: 569–579. doi:10.4319/lo.2000.45.3.0569

Mitra, A., and others. 2016. Defining planktonic protist functional groups on mechanisms for energy and nutrient acquisition: Incorporation of diverse Mixotrophic strategies. Protist **167**: 106–120. doi:10.1016/j.protis.2016.01.003

Mruwat, N., and others. 2021. A single-cell polony method reveals low levels of infected *Prochlorococcus* in oligotrophic waters despite high cyanophage abundances. ISME J. **15**: 41–54. doi:10.1038/s41396-020-00752-6

Pasulka, A. L., M. R. Landry, D. A. Taniguchi, A. G. Taylor, and M. J. Church. 2013. Temporal dynamics of phytoplankton and heterotrophic protists at station ALOHA. Deep-Sea Res. II Top. Stud. Oceanogr. **93**: 44–57. doi:10.1016/j.dsr2.2013.01.007

Poff, K. E., A. O. Leu, J. M. Eppley, D. M. Karl, and E. F. DeLong. 2021. Microbial dynamics of elevated carbon flux in the open ocean's abyss. Proc. Natl. Acad. Sci. USA **118**: e2018269118. doi:10.1073/pnas.2018269118

Ribalet, F., J. Swalwell, S. Clayton, V. Jiménez, S. Sudek, Y. Lin, Z. I. Johnson, A. Z. Worden, and E. V. Armbrust. 2015. Light-driven synchrony of *Prochlorococcus* growth and mortality in the subtropical Pacific gyre. Proc. Natl. Acad. Sci. USA **112**: 8008–8012. doi:10.1073/pnas.1424279112

Ribalet, F., and others. 2019. Seaflow data v1, high-resolution abundance, size and biomass of small phytoplankton in the North Pacific. Sci. Data **6**: 1–8. doi:10.1038/s41597-019-0292-2

Rii, Y. M., D. M. Karl, and M. J. Church. 2016. Temporal and vertical variability in picophytoplankton primary productivity in the North Pacific Subtropical Gyre. Mar. Ecol. Prog. Ser. **562**: 1–18. doi:10.3354/meps11954

Rii, Y. M., L. M. Peoples, D. M. Karl, and M. J. Church. 2022. Seasonality and episodic variation in picoeukaryote diversity and structure reveal community resilience to disturbances in the North Pacific Subtropical Gyre. Limnol. Oceanogr. **67**: 5331–5351. doi:10.1002/lno.11916

Sakamoto, C. M., D. M. Karl, H. W. Jannasch, R. R. Bidigare, R. M. Letelier, P. M. Walz, J. P. Ryan, P. S. Polito, and K. S. Johnson. 2004. Influence of Rossby waves on nutrient dynamics and the plankton community structure in the North Pacific subtropical gyre. J. Geophys. Res. **109**: C05032. doi:10.1029/2003JC001976

Scharek, R., M. Latasa, D. M. Karl, and R. R. Bidigare. 1999. Temporal variations in diatom abundance and downward vertical flux in the oligotrophic North Pacific gyre. Deep Sea Res. I Oceanogr. Res. Pap. **46**: 1051–1075. doi:10.1016/S0967-0637(98)00102-2

Shalapyonok, A., R. J. Olson, and L. S. Shalapyonok. 1998. Ultradian growth in *Prochlorococcus* spp. Appl. Environ. Microbiol. **64**: 1066–1069. doi:10.1128/aem.64.3.1066-1069.1998

Shi, D., W. Li, B. M. Hopkinson, H. Hong, D. Li, S.-J. Kao, and W. Lin. 2015. Interactive effects of light, nitrogen source, and carbon dioxide on energy metabolism in the diatom *Thalassiosira pseudonana*. Limnol. Oceanogr. **60**: 1805–1822. doi:10.1002/lno.10134

Swalwell, J. E., F. Ribalet, and E. V. Armbrust. 2011. SeaFlow: A novel underway flow-cytometer for continuous observations of phytoplankton in the ocean. Limnol. Oceanogr.: Methods **9**: 466–477. doi:10.4319/lom.2011.9.466

Thaben, P. F., and P. O. Westermark. 2014. Detecting rhythms in time series with RAIN. J. Biol. Rhythms **29**: 391–400. doi:10.1177/0748730414553029

Vaulot, D., C. Courties, and F. Partensky. 1989. A simple method to preserve oceanic phytoplankton for flow cytometric analyses. Cytometry **10**: 629–635. doi:10.1002/cyto.990100519

Vaulot, D., D. Marie, R. J. Olson, and S. W. Chisholm. 1995. Growth of *Prochlorococcus*, a photosynthetic prokaryote, in the Equatorial Pacific Ocean. Science **268**: 1480–1482. doi:10.1126/science.268.5216.1480

Vaulot, D., and D. Marie. 1999. Diel variability of photosynthetic picoplankton in the equatorial Pacific. J. Geophys. Res. **104**: 3297–3310. doi:10.1029/98JC01333

Villareal, T. A., C. G. Brown, M. A. Brzezinski, J. W. Krause, and C. Wilson. 2012. Summer diatom blooms in the North Pacific Subtropical Gyre: 2008–2009. PLoS One **7**: e33109. doi:10.1371/journal.pone.0033109

Ward, B. A., and M. J. Follows. 2016. Marine mixotrophy increases trophic transfer efficiency, mean organism size, and vertical carbon flux. Proc. Natl. Acad. Sci. USA **113**: 2958–2963. doi:10.1073/pnas.1517118113

White, A. E., Y. H. Spitz, and R. M. Letelier. 2007. What factors are driving summer phytoplankton blooms in the

North Pacific Subtropical Gyre? J. Geophys. Res. **112**: C12006. doi:10.1029/2007JC004129

White, A. E., R. M. Letelier, A. L. Whitmire, B. Barone, R. R. Bidigare, M. J. Church, and D. M. Karl. 2015. Phenology of particle size distributions and primary productivity in the North Pacific subtropical gyre (Station ALOHA). J. Geophys. Res. Oceans **120**: 7381–7399. doi:10.1002/2015JC010897

White, A. E., B. Barone, R. M. Letelier, and D. M. Karl. 2017. Productivity diagnosed from the diel cycle of particulate carbon in the North Pacific Subtropical Gyre. Geophys. Res. Lett. **44**: 3752–3760. doi:10.1002/2016GL071607

Wilson, S. T., and others. 2015. Short-term variability in euphotic zone biogeochemistry and primary productivity at Station ALOHA: A case study of summer 2012. Global Biogeochem. Cycles **29**: 1145–1164. doi:10.1002/2015GB005141

Wilson, S. T., and others. 2017. Coordinated regulation of growth, activity and transcription in natural populations of the unicellular nitrogen-fixing cyanobacterium *Crocosphaera*. Nat. Microbiol. **2**: 1–9. doi:10.1038/nmicrobiol.2017.118

Winn, C. D., L. Campbell, J. R. Christian, R. M. Letelier, D. V. Hebel, J. E. Dore, L. Fujieki, and D. M. Karl. 1995. Seasonal variability in the phytoplankton community of the North Pacific Subtropical Gyre. Global Biogeochem. Cycles **9**: 605–620. doi:10.1029/95GB02149

Xie, Y., E. A. Laws, L. Yan, and B. Huang. 2018. Diel patterns of variable fluorescence and carbon fixation of picocyanobacteria *Prochlorococcus*-dominated phytoplankton in the South China Sea basin. Front. Microbiol. **9**: 1589. doi:10.3389/fmicb.2018.01589

Acknowledgments

We would like to thank the HOT and SCOPE-Ops teams, particularly T. Burrell and R. Tabata for operating the SeaFlow during HOT cruises. Thanks to M. Church for discussions on biomass, productivity, and diazotrophy and to three anonymous reviewers for their comments. This work was supported by grants from the Simons Foundation (Award IDs #574495 to FR, #723795 to EVA, and #329104 to AEW). The HOT program is supported by the National Science Foundation (# NSF OCE 1756517 to AEW).

Conflict of Interest

None declared.

Submitted 01 November 2023
Revised 12 April 2024
Accepted 23 August 2024

Associate editor: Bingzhang Chen